Pergamon PII: S0038–092X(00)00014–1
www.elsevier.com/locate/solener
Solar Energy Vol. 69, No. 1, pp. 55–66, 2000

0038-092X/00/$ - see front matter

NUMERICAL SIMULATION AND SENSITIVITY ANALYSIS OF LATTICE PASSIVE SOLAR HEATING WALLS

XIANDE FANG*,† and YUANZHE LI**
*Institute of Air Conditioning and Refrigeration, Nanjing University of Aeronautics and Astronautics, Nanjing 210016, People's Republic of China
**Department of Thermal Engineering, Tsinghua University, Beijing, People's Republic of China

Received 14 December 1998; revised version accepted 27 October 1999

Communicated by ANDREAS ATHIENITIS

Abstract—A lattice passive solar heating wall (LPSHW) can remarkably improve the heating performance of passive solar heated buildings. Many parameters affect the thermal performance of the LPSHW so that it is not realistic to scrutinize the thermal performance of the LPSHW experimentally. This paper develops a three-dimensional transient heat transfer model of the LPSHW, based on which a computer simulation program is developed in FORTRAN language. The model predictions agree quite well with experimental data. The program can be used to simulate and evaluate the transient thermal performance, to analyze the sensitivity and the effect of climate, and to optimize LPSHW structural parameters. Hour-by-hour computer simulations are run with the program to analyze the sensitivity of a variety of parameters of the LPSHW. The calculations are rerun many times with structural parameters changed one at a time so that the effect of the changed structural parameter on the thermal performance of the LPSHW can be assessed. From the sensitivity analysis, the optimum configuration is thus obtained. The comparison between the LPSHW and the Trombe wall is made thereafter. Under the chosen conditions, thermal efficiency is 30.2% for the LPSHW and 22.6% for the Trombe wall.

1. INTRODUCTION

Using a lattice wall as the thermal storage wall of a passive solar heated building yields a new type of solar wall, defined as a lattice passive solar heating wall (LPSHW). A passive solar heated building with an LPSHW (Fig. 1a) is defined as a lattice-wall passive solar heated building.

In the winter of 1981, a farmer′s house at Daxin County, Beijing was retrofitted into a passive solar heated house. Several kinds of thermal storage walls, including the Trombe wall, were constructed to run comparison tests. The experimental data showed that the lattice-wall passive solar heated room had better thermal performance, less material consumption, and a more beautiful style than the Trombe-wall passive solar heated room (Li *et al*., 1985). Four test cells were built side-by-side in Tsinghua University in 1983 to conduct performance tests on the LPSHW. Comparison tests between the LPSHW and the Trombe wall confirmed the conclusion that the LPSHW has more advantages over the Trombe wall (Fang, 1984). Now, the LPSHW is used more than any other storage wall in China when a solar wall is built under a direct gain window.

The LPSHW, which is usually used as the southern wall of the passive solar heated building, consists of a lattice wall and a glazing cover. The lattice wall is usually made of bricks or concrete blocks, placed about 50–100 mm from behind the glazing cover. The configuration of the lattice wall is much more complicated than that of the Trombe wall. A typical lattice wall has rectangular vents which are equal in size and are distributed uniformly (Fig. 1), while a Trombe wall may have no vents or have vents only at the top and bottom of the wall (Balcomb *et al*., 1977).

For designing a lattice-wall passive solar heated building, it is necessary to determine LPSHW structural parameters. Experiments are not able to fully explain the thermal performance of the LPSHW because it is influenced by so many parameters (Fang, 1986), such as the thickness, height, thermal conductivity, and surface emissivity of the lattice wall, the area and distribution of lattice wall vents, as well as glazing cover parameters. Therefore, computer simulation is needed.

†Author to whom correspondence should be addressed. Tel.: +86-25-4892853; e-mail: xdfang@;lonline.com

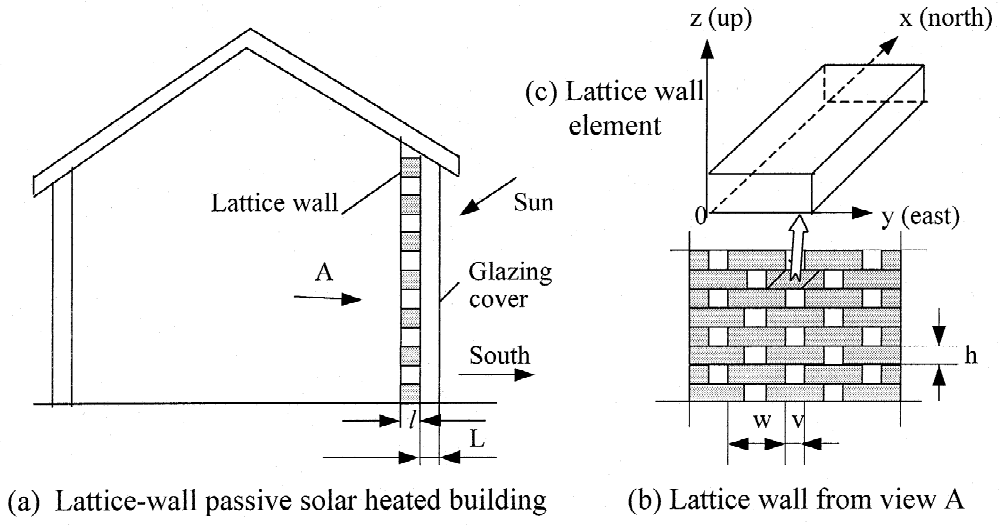

Fig. 1. Lattice wall and lattice-wall passive solar heated building.

It is difficult to develop the computer simulation program not only because of the complicated configuration of the LPSHW, but also because of complicated heat transfer boundary conditions. Sunlight passes through the glazing cover and irradiates on some part of the lattice wall surface, yielding irregular heat flow boundary conditions. Complicated convection boundary conditions occur because air flows through the vents and the channel between the lattice wall and the glazing cover. In addition, multiple-surface thermal radiation conditions exist. Consequently, the remarkable difference of heat transfer boundary conditions of each side of the lattice wall makes it necessary to consider the heat conduction in the lattice wall to be three-dimensional.

For the numerical simulation of the LPSHW, no previous results have been found. Our work includes the following five main parts:

1. mathematical model of air flow through lattice wall vents and the channel between the lattice wall and the glazing cover;
2. mathematical model of three-dimensional transient heat conduction in the lattice wall;
3. mathematical model of the building envelope in addition to the LPSHW;
4. development of the computer program;
5. sensitivity analysis and optimization.

Part (1) was introduced in a previous paper (Fang, 1984) and is summarized in Appendix A. Part (3) is much simpler than part (2), and is developed in a similar way so that it will not be discussed here. This paper focuses on parts (2), (4), and (5).

2. DIFFERENTIAL EQUATIONS OF A LATTICE WALL

The governing equation of heat conduction in a lattice wall is given by

$$\frac{\partial^2 T}{\partial x^2}+\frac{\partial^2 T}{\partial y^2}+\frac{\partial^2 T}{\partial z^2}=\frac{1}{a}\frac{\partial T}{\partial \tau}. \tag{1}$$

A block separated from a lattice wall (Fig. 1c) is defined as a lattice wall element. Each lattice wall element has the same configuration, the same heat flow boundary conditions, and the same thermal radiation boundary conditions, but the convection boundary conditions are different from each other. Generally, the temperature and velocity of the air in lattice wall vents and the channel between the lattice wall and the glazing cover vary with wall altitude. The correlation of the temperature and velocity of the air in lattice wall vents and the channel varying with wall altitude has been developed (Fang, 1984; summarized in Appendix A), which makes it practical to choose a lattice wall element as the physical model for developing the mathematical model of a lattice wall.

A lattice wall element has six sides, i.e. $x = 0$, $x = l$, $y = 0$, $y = w$, $z = 0$, and $z = h$. All the sides are exposed to air except for the isolated surfaces. An isolated surface is created by isolating a lattice wall element from the lattice wall. Therefore, only the sides $z = 0$ and $z = h$ have isolated surfaces.

The following assumptions are made for developing the differential equations of the boundary surfaces of a lattice wall element.

1. The heat conduction through isolated surfaces is neglected.
2. For a given side, heat transfer coefficients are the same, while different sides have different heat transfer coefficients.
3. Solar radiation on a side is uniformly distributed.

For a lattice wall element in row k ($k = 1$ for the bottom row, and $k = M$ for the top row), the mathematical model of the boundary surfaces is as follows:

$$-\lambda\frac{\partial T(x,y,z)}{\partial x}\bigg|_{x=0} = I_x + h_{sc}[T_c(k) - T(0,y,z)] + h_{sr}[T_g - T(0,y,z)] \quad (2a)$$

$$-\lambda\frac{\partial T(x,y,z)}{\partial x}\bigg|_{x=l} = h_{nc}[T(l,y,z) + T_r] + h_{sr}[T(l,y,z) - T_w] \quad (2b)$$

$$-\lambda\frac{\partial T(x,y,z)}{\partial y}\bigg|_{y=0} = I_{ya} + h_{vc}(k)[T_v(k) - T(x,0,z)] + h_{vwr}[T_w - T(x,0,z)] + h_{vgr}[T_g - T(x,0,z)] \quad (2c)$$

$$\lambda\frac{\partial T(x,y,z)}{\partial y}\bigg|_{y=w} = I_{yb} + h_{vc}(k)[T_v(k) - T(x,w,z)] + h_{vwr}[T_w - T(x,w,z)] + h_{vgr}[T_g - T(x,w,z)] \quad (2d)$$

$$-\lambda\frac{\partial T(x,y,z)}{\partial z}\bigg|_{z=0} = \frac{v}{w}\{h_{vc}(k-1)[T_v(k-1) - T(x,y,0)] + h_{vwr}[T_w - T(x,y,0)] + h_{vgr}[T_g - T(x,y,0)]\} \quad (2e)$$

and

$$\lambda\frac{\partial T(x,y,z)}{\partial z}\bigg|_{z=h} = \frac{v}{w}\{I_{yb} + h_{vc}(k+1)[T_v(k+1) - T(x,y,h)] + h_{vwr}[T_w - T(x,y,h)] + h_{vgr}[T_g - T(x,y,h)]\} \quad (2f)$$

where, h_{nc} is calculated according to natural convection on vertical plates (Incropera and DeWitt, 1996), h_{sc} is given by Utzinger *et al.* (1968), and h_{vc} is given by Metais and Eckert (1964).

3. FINITE-DIFFERENCE EQUATIONS OF A LATTICE WALL

Two kinds of thermal nodal networks are used to develop the finite-difference equation of a lattice wall. One is the rectangular thermal nodal network that is widely used in numerical heat transfer. The other is the hybrid thermal nodal network as shown in Fig. 2.

This paper is concentrated on the hybrid thermal nodal network. For an arbitrary temperature node $T(i,j,k)$, i denotes the number of the nodal points in the x direction, j denotes the number of the nodal points of the $y-z$ plane, and k denotes the row number of the lattice wall element. For each node i, there are five nodes on the $y-z$ plane, which are numbered $j = 1$, 2, 3, 4, and 5, respectively (Fig. 2).

For a $y-z$ plane, five nodes are enough because the area of the $y-z$ plane of a lattice wall element should not be large, and the temperature gradients in the y and z directions are much less than that in the x direction. Compared with the rectangular thermal nodal network, the hybrid type saves a lot of computing time and storage units.

The implicit and explicit finite-difference meth-

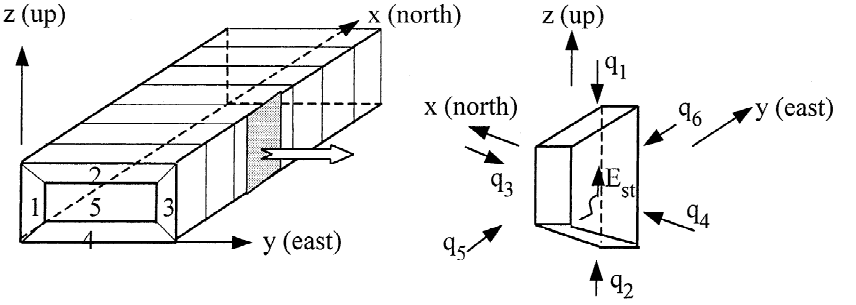

(a) Thermal nodal network (b) Energy balance of the control volume

Fig. 2. Thermal nodal network of a lattice wall element.

ods were widely used for simulating passive solar heated buildings (Balcomb *et al*., 1977; Li *et al*., 1983; Carter, 1990). These methods have only the first-order time accuracy. In order to achieve more accurate simulation results, this paper uses the Crank–Nicolson method (Crank and Nicolson, 1947; Roache, 1972; Welty, 1978), which has the second-order time accuracy. The energy balance method is used for developing the finite-difference equation.

The detail of the development of the finite-difference equations is not described here because it is complicated. At first, we take nodal point $T(i,3,k)$ for example to show the method. Then the finite-difference equations of an arbitrary nodal point $T(i,j,k)$ are given directly.

Referring to Fig. 2b, the energy balance equation of nodal point (i, 3, k) is

$$(q_1 + q_2) + (q_3 + q_4) + (q_5 + q_6) = E_{\mathrm{st}} \tag{3}$$

where the left of the equation is total heat gain of the control volume at time $(n + 1/2)\Delta\tau$, and the right, E_{st}, is the internal energy augment during the period of $(n + 1)\Delta\tau - n\Delta\tau$. Letting $\Delta y = w/2$ and $\Delta z = h/2$, we obtain

$$\begin{aligned} q_1 + q_2 = \frac{\lambda}{\Delta z}\cdot\frac{\Delta x\Delta y}{2}\Big\{&\frac{1}{2}\big[T(i,2,k) + T(i,4,k) \\ &- 2T(i,3,k)\big] + \frac{1}{2}\big[T^0(i,2,k) + T^0(i,4,k) \\ &- 2T^0(i,3,k)\big]\Big\} \end{aligned} \tag{4}$$

$$\begin{aligned} q_3 + q_4 = \frac{\lambda}{\Delta x}\cdot\frac{3\Delta z\Delta y}{4}\Big\{&\frac{1}{2}\big[T(i-1,3,k) \\ &+ T(i+1,3,k) - 2T(i,3,k)\big] \\ &+ \frac{1}{2}\big[T^0(i-1,3,k) + T^0(i+1,3,k) \\ &- 2T^0(i,3,k)\big]\Big\} \end{aligned} \tag{5}$$

$$\begin{aligned} q_5 + q_6 = \frac{\lambda}{\Delta y}\cdot\Delta x\Delta z\Big\{&\frac{1}{2}\big[T(i,5,k) - T(i,3,k)\big] \\ &+ \frac{1}{2}\big[T^0(i,5,k) - T^0(i,3,k)\big] \\ &+ 2\Big\{\frac{1}{2}\big\{I_{ya} + h_{\mathrm{vc}}(k)\big[T_{\mathrm{v}}(k) - T(i,3,k)\big] \\ &+ h_{\mathrm{vgr}}\big[T_{\mathrm{g}} - T(i,3,k)\big] \\ &+ h_{\mathrm{vwr}}\big[T_{\mathrm{w}} - T(i,3,k)\big]\Big\} + 2\Big\{\frac{1}{2}\big\{I^0_{ya} \\ &+ h^0_{\mathrm{vc}}(k)\big[T^0_v(k) - T^0(i,3,k)\big] \\ &+ h^0_{\mathrm{vgr}}\big[T^0_g - T^0(i,3,k)\big] \\ &+ h^0_{\mathrm{vwr}}\big[T^0_w - T^0(i,3,k)\big]\big\}\Big\} \end{aligned} \tag{6}$$

and

$$E_{\mathrm{st}} = \frac{3}{4}\cdot\Delta x\Delta y\Delta z\cdot\frac{\rho c}{\Delta\tau}\big[T(i,3,k) - T^0(i,3,k)\big] \tag{7}$$

where T, h, and I (without superscripts) denote the temperatures, heat transfer coefficients, and solar radiation fluxes at time $(n + 1)\Delta\tau$, respectively, and T^0, h^0, and I^0 denote the temperatures, heat transfer coefficients, and solar radiation fluxes at time $n\Delta\tau$, respectively.

Substituting for the heat gains from Eqs. (4)–(6) and for the internal energy augment from Eq. (7), Eq. (3) will become the finite-difference equation at nodal point (i,3,k). Using the method just mentioned, the finite-difference equation at an arbitrary nodal point (i,j,k) is then of the form:

$$T(i,j,k) = \frac{f(i,j,k) + B(i,j,k)}{B_a(i,j,k)} \tag{8}$$

where

$$f(i,j,k) = AT_{xt} + C(T_{yt} + T_{zt}) \tag{9}$$

$$B_a(i,j,k) = AT_{xc} + C(T_{yc} + T_{zc} + P) \tag{10}$$

and

$$\begin{aligned} B = AS_x + CS_{yz} + \left[\frac{4AC}{F_0} - B_a(i,j,k)\right]T^0(i,j,k) \\ + f^0(i,j,k) \end{aligned} \tag{11}$$

where

$$A = \begin{cases} 3/4 & \text{for} \quad j < 5 \\ 1 & \text{for} \quad j = 5 \end{cases} \tag{12}$$

$$C = \begin{cases} 1/2 & \text{for} \quad i = 1, N_x \\ 1 & \text{for} \quad 1 < i < N_x \end{cases} \tag{13}$$

$$T_{xt} = \begin{cases} \dfrac{l^2}{\lambda\Delta x}[h_{\mathrm{sc}}T_{\mathrm{c}}(k) + h_{\mathrm{sr}}T_{\mathrm{g}}] + \left(\dfrac{l}{\Delta x}\right)^2 T(i,j,k) & i = 1 \\ \left(\dfrac{l}{\Delta x}\right)^2 [T(i-1,j,k) + T(i+1,j,k)] & 1 < i < N_x \\ \dfrac{l^2}{\lambda\Delta x}[h_{\mathrm{nc}}T_{\mathrm{r}}(k) + h_{\mathrm{nr}}T_{\mathrm{w}}] + \left(\dfrac{l}{\Delta x}\right)^2 T(N_x - 1,j,k) & i = N_x \end{cases} \tag{14}$$

$$T_{yt} = \begin{cases} \dfrac{2l^2}{\lambda\Delta y}[h_{\mathrm{vc}}(k)T_{\mathrm{v}}(k) + h_{\mathrm{vwr}}T_{\mathrm{w}} + h_{\mathrm{vgr}}T_{\mathrm{g}}] + \left(\dfrac{l}{\Delta y}\right)^2 T(i,5,k) & j = 1,3 \\ 0.5\left(\dfrac{l}{\Delta y}\right)^2 [T(i,1,,k) + T(i,3,k)] & j = 2,4 \\ \left(\dfrac{l}{\Delta y}\right)^2 [T(i,1,,k) + T(i,3,k)] & j = 5 \end{cases} \tag{15}$$

$$T_{zt} = \begin{cases} 0.5\left(\frac{l}{\Delta z}\right)^2 [T(i,2,,k) + T(i,4,k)] & j = 1,3 \\ \frac{2vl^2}{\lambda w \Delta z}[h_{vc}(k+1)T_v(k+1) + h_{vwr}T_w + h_{vgr}T_g] + \left(\frac{l}{\Delta z}\right)^2 T(i,5,k) & j = 2 \\ \frac{2vl^2}{\lambda w \Delta z}[h_{vc}(k-1)T_v(k-1) + h_{vwr}T_w + h_{vgr}T_g] + \left(\frac{l}{\Delta z}\right)^2 T(i,5,k) & j = 4 \\ \left(\frac{l}{\Delta z}\right)^2 [T(i,2,,k) + T(i,4,k)] & j = 5 \end{cases} \quad (16)$$

$$T_{xc} = \begin{cases} \frac{l^2}{\lambda \Delta x}(h_{sc} + h_{sr}) & i = 1 \\ 0 & 1 < i < N_x \\ \frac{l^2}{\lambda \Delta x}(h_{nc} + h_{nr}) & i = N_x \end{cases} \quad (17)$$

$$T_{yc} = \begin{cases} \frac{2l^2}{\lambda \Delta y}[h_{vc}(k) + h_{vwr} + h_{vgr}] & j = 1,3 \\ 0 & j = 2,4,5 \end{cases} \quad (18)$$

$$T_{zc} = \begin{cases} 0 & j = 1,3,5 \\ \frac{2vl^2}{\lambda w \Delta z}[h_{vc}(k+1) + h_{vwr} + h_{vgr}] & j = 2 \\ \frac{2vl^2}{\lambda w \Delta z}[h_{vc}(k-1) + h_{vwr} + h_{vgr}] & j = 4 \end{cases} \quad (19)$$

$$S_x = \begin{cases} \frac{l^2}{\lambda \Delta x}(I_x + I_x^0) & i = 1 \\ 0 & i > 1 \end{cases} \quad (20)$$

$$S_{yz} = \begin{cases} \frac{2l^2}{\lambda \Delta y}(I_{ya} + I_{ya}^0) & j = 1 \\ \frac{2vl^2}{\lambda w \Delta z}(I_z + I_z^0) & j = 2 \\ \frac{2l^2}{\lambda \Delta y}(I_{yb} + I_{yb}^0) & j = 3 \\ 0 & j = 4,5 \end{cases} \quad (21)$$

and

$$P = \begin{cases} 2\left[\frac{1}{F_0} + \left(\frac{l}{\Delta x}\right)^2 + \left(\frac{l}{\Delta y}\right)^2 + \left(\frac{l}{\Delta z}\right)^2\right] & j = 5 \\ \frac{1.5}{F_0} + 1.5\left(\frac{l}{\Delta x}\right)^2 + \left(\frac{l}{\Delta y}\right)^2 + \left(\frac{l}{\Delta z}\right)^2 & j \neq 5 \end{cases} \quad (22)$$

In the development of the thermal nodal point equations of the interior surfaces of a building envelope and glazing cover, average radiation temperatures of the lattice wall are needed. They can be determined based on the weighted average method with the related nodal point area as the weight, as described in Appendix B.

4. COMPUTER SIMULATION PROGRAM

The mathematical model of a lattice-wall passive solar heated building consists of the mathematical model of the lattice wall, the air flow through lattice wall vents and the channel between the lattice wall and the glazing cover, the building envelope, and the solar gain. Based on the mathematical model of lattice-wall passive solar heated buildings, a computer simulation program in FORTRAN language is developed. The program is composed of one main procedure and nine subroutine procedures.

The G-S reiteration method is used to solve the governing equations. The coefficients of the equations are dependent on current temperatures so that the equations are nonlinear. In order to use the G-S reiteration method, it is necessary to convert the nonlinear equations to linear ones. For this reason, a reiterating process at time $(n+1)\Delta\tau$ is divided into several reiterating sub-processes. At the beginning of the first reiterating sub-process, the temperatures at time $n\Delta\tau$ are used to calculate the equation coefficients. Then, the first reiterating sub-process is run with a given error range of the temperatures as stop sign, keeping all the coefficients constant. When all the reiterating errors go in the given error range, the first reiterating sub-process ends, and the second reiterating sub-process begins. At the beginning of the second reiterating sub-process, the calculating data of the first reiterating sub-process are used to calculate the equation coefficients. The second sub-process is run in the same way as the first reiterating sub-process. Satisfied results for a reiterating process are achieved after all the reiterating sub-processes are run. With the method just described, the nonlinear issue becomes a linear one.

The program is verified with experimental data (Fang, 1984). The experiments were performed with four side-by-side test rooms with the inner space of length$\times$depth$\times$height$=1.2\times1\times1$ m^3. There are no internal auxiliary heat sources so that the test rooms operated naturally. The envelopes of the test rooms are composed of polyfoam plates. Fig. 3 shows the ambient temperature and solar radiation during the experimental period. Figs. 4–6 compare the model predictions with the experimental data. The satisfactory predicting accuracy is owed mainly to the following aspects:

1. three dimensional heat conduction model for the lattice wall;
2. transient heat transfer coefficients for all the governing equations;

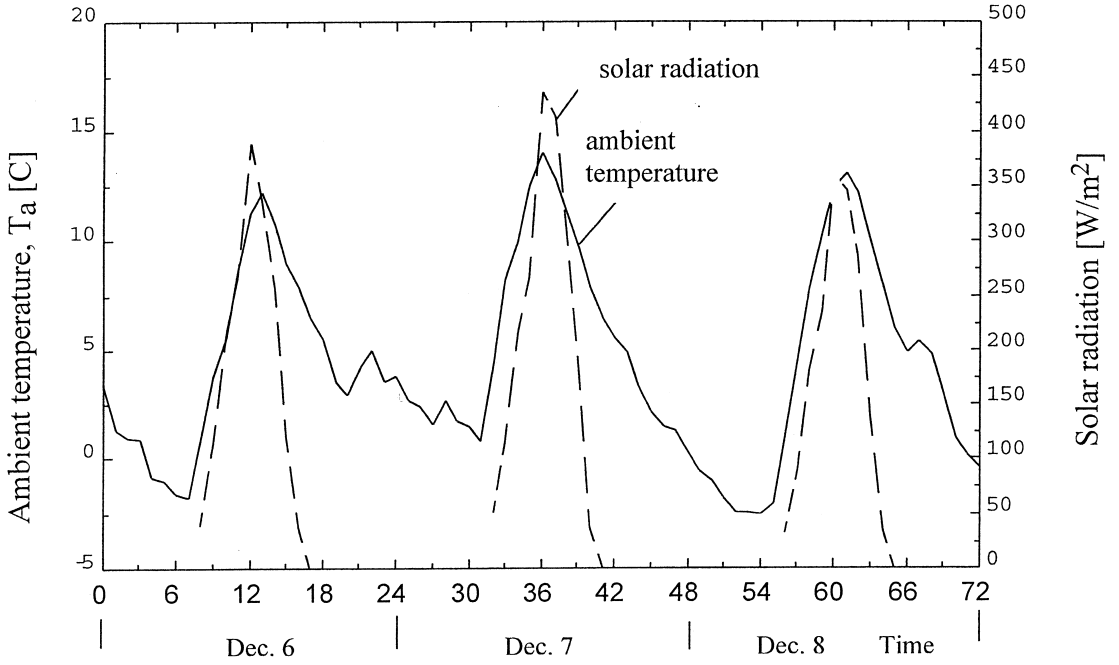

Fig. 3. Ambient temperature and the solar radiation on southern wall.

3. use of the Crank–Nicolson method. For the hour-by-hour simulation under variable weather conditions, this method improves the simulation accuracy remarkably.

Referring to Figs. 5 and 6, T_r is greater than $T_{x=l}$ during most of the daytime. This means that all the exposed surfaces of the lattice wall collect solar energy during that time. Convection, which makes energy transfer from the Trombe wall to air during all the operating time, now is a means

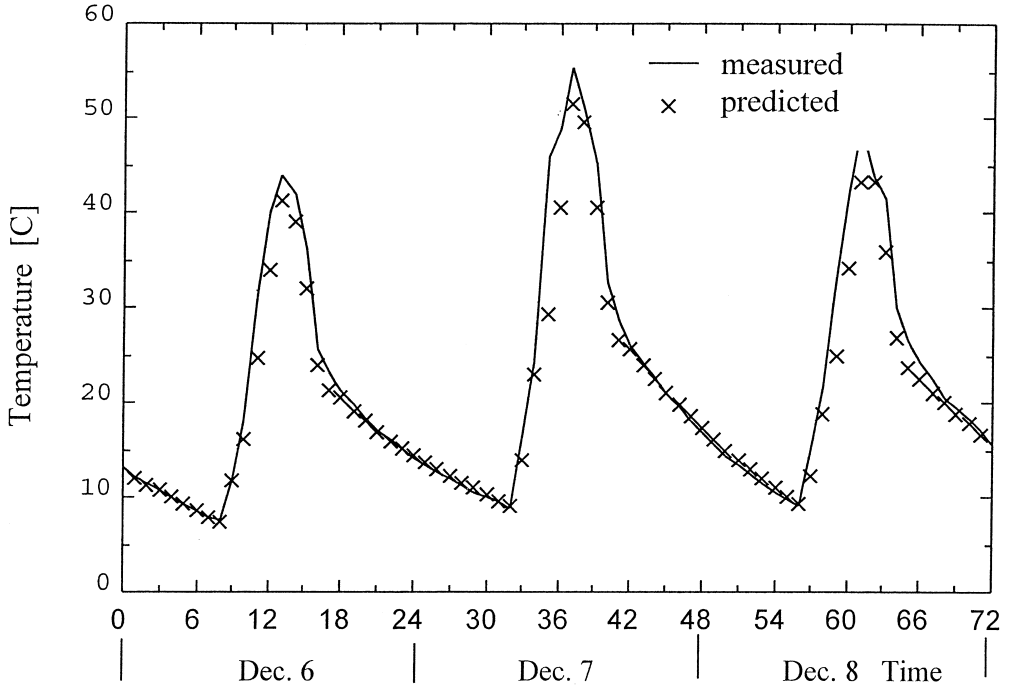

Fig. 4. Lattice wall temperature ($x = 0$ side): predicted vs. measured.

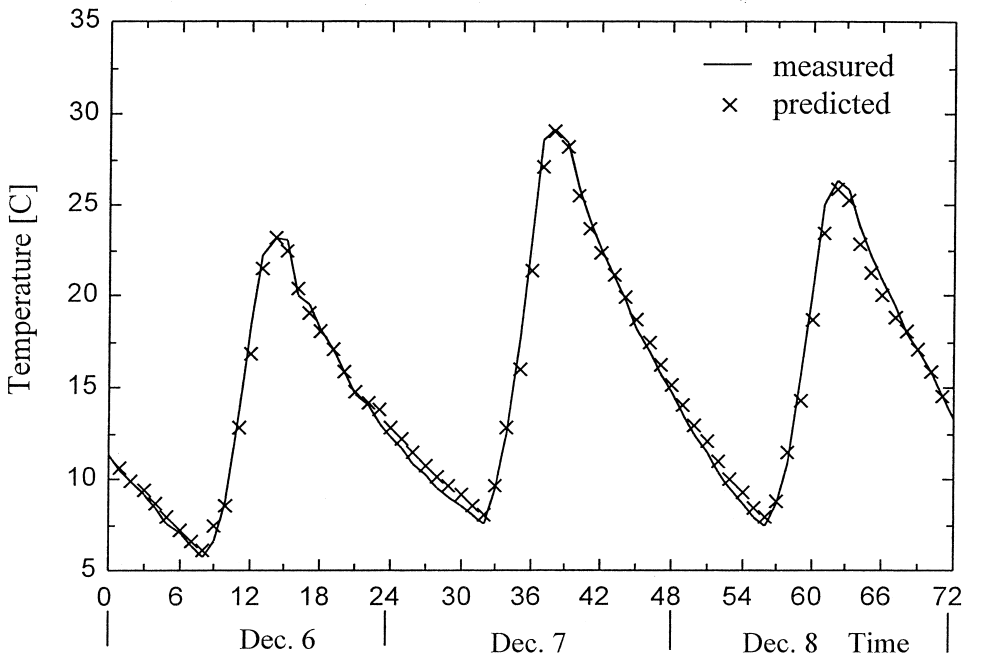

Fig. 5. Room temperature: predicted vs. measured.

for the lattice wall to collect solar energy. Accordingly, the LPSHW has higher thermal efficiency than the Trombe wall if other conditions are the same. The fluctuation of the room temperature is a little greater than that of the wall interior-surface temperature, and much greater than that of the ambient temperature. This is partly because of the convection by lattice wall vents, partly because of the light envelopes of the test rooms, and partly because of no internal auxiliary heat sources.

The program can be used to simulate and evaluate the transient thermal performance, to

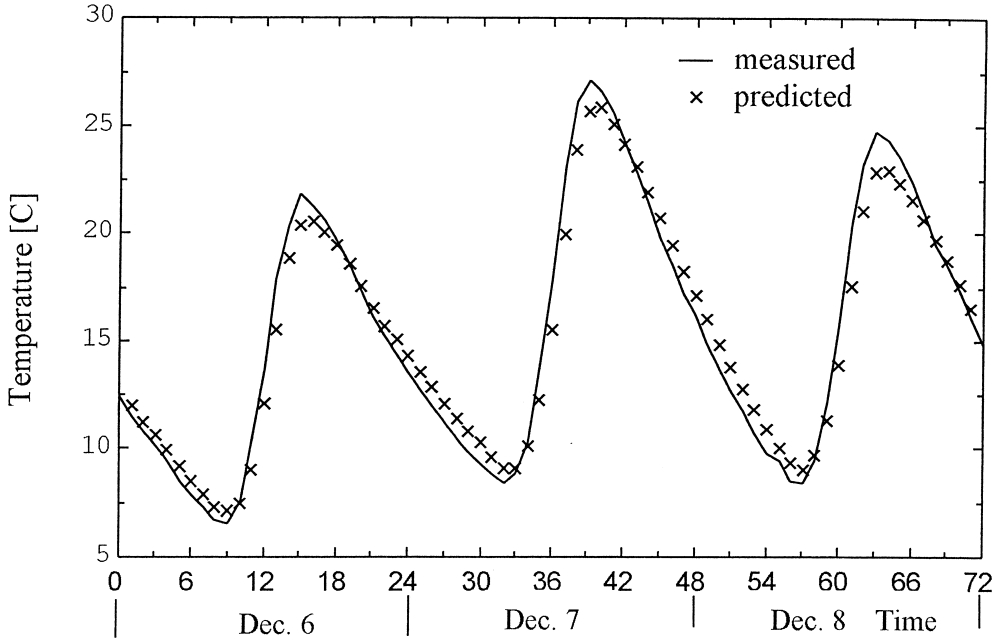

Fig. 6. Lattice wall temperature ($x = l$ side): predicted vs. measured.

analyze the sensitivity and the effect of climate, and to study the optimum structural parameters of the LPSHW.

5. SENSITIVITY ANALYTICAL PROCEDURE

To analyze the sensitivity of the LPSHW, hour-by-hour calculations are run and repeated many times with structural parameters changed one at a time.

The parameters include the glazing layer number, lattice wall height H, night insulation value R, wall thickness l, vent height h, and the porosity P_o defined by Eq. (23). Both single glazing and double glazing are considered. The wall height includes 1 m and 3 m. The former denotes the wall used under direct gain windows, and the latter stands for a normal height wall

$$P_o = \frac{\text{the total area of the vents of a lattice wall}}{\text{the lattice wall height} \times \text{the lattice wall width}}. \quad (23)$$

The heating performance of a passive solar heated building can be evaluated with a comprehensive heating index (CHI), which is dependent on the thermal efficiency η defined by Eq. (24), the emphatic heating period thermal efficiency η' defined by Eq. (26), and the stability S defined by Eq. (27) (Li *et al*., 1989).

$$\eta = \frac{\text{LCR} \times (\text{mean room temperature} - \text{mean ambient temperature})}{\text{the total solar radiation incident on the glazing cover}} \quad (24)$$

where LCR is given by

$$\text{LCR} = \frac{\text{per unit of inside/outside temperature difference}}{\text{the area of the glazing cover}} \quad (25)$$

$$\eta' = \frac{\text{LCR} \times \text{mean room/ambient temperature difference during the emphatic heating period of a day}}{\text{the total solar radiation incident on the glazing cover}} \quad (26)$$

$$S = 2\left|q_{T_{ex}} - q_{T_{ex-1}}\right| / \left(q_{T_{ex}} + q_{T_{ex-1}}\right). \quad (27)$$

For a dwelling house, CHI can be given by

$$\text{CHI} = 0.05\eta + 0.85\eta' + 0.1S. \quad (28)$$

Middle clear solar/weather data in Beijing in January are chosen for the calculation. The total daily solar radiation intensity is 2760.3 Wh m^{-2}, and the maximum solar radiation flux is 473.3 W m^{-2}. The ambient temperature fluctuates between -8.7°C and 2.7°C with average -4°C.

Some parameters used for the sensitivity analysis are as follows: LCR = 2.4 W m^{-2} °C^{-1}; no auxiliary heat; ground reflectance = 0.19, isotropic; vertical glass, south-facing by east 10 degree; absorptivity of the building envelope = 0.71. Thermal storage wall properties:

1. Concrete wall
   Thermal diffusivity = 0.0025 m^2 h^{-1}
   Thermal conductivity = 1.28 W m^{-1} °C^{-1}
   Absorptivity = 0.96
2. Brick wall
   Thermal diffusivity = 0.00184 m^2 h^{-1}
   Thermal conductivity = 0.81 W m^{-1} °C^{-1}
   Absorptivity = 0.96

Night insulation time: from 16:00 h to 08:00 h.

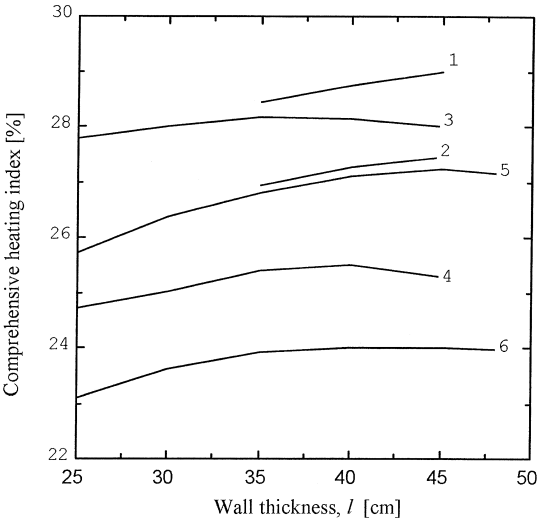

Fig. 7. Effect of wall thickness on thermal performance.

6. SENSITIVITY ANALYSIS

The following sensitivity analysis is based on Eq. (28), which is used for evaluating dwelling passive solar heated buildings.

6.1. Effect of wall thickness l

Fig. 7 illustrates the effect of the wall thickness on the thermal performance of the LPSHW. In addition to the parameters given above and in Table 1, some other parameters in Fig. 7 are $h = 6$ cm, $P_o = 0.35$ for the 3-m-high walls, and $P_o = 0.4$ for the 1-m-high walls.

Table 1. Some parameters in Figs. 7 and 8

Curve number	Material	H, m	Glazing layer	R, m^2 °C W^{-1}
1	Concrete	3	Double	1.25
2	Concrete	3	Single	1.25
3	Concrete	1	Single	1.25
4	Concrete	1	Single	0.33
5	Brick	1	Single	1.25
6	Brick	1	Single	0.33

For a low brick wall ($H=1$ m), as used under a direct gain window, and a normal height wall ($H=3$ m), the performances generally improve with their thickness increasing within engineering applications. For a low concrete wall, there is an optimum thickness. The preferable wall thickness increases with increasing wall height for a given wall material, and decreases with increasing wall thermal conductivity for a given wall height.

Brick walls with thickness 49 cm show the best performance, but they are too thick from an engineering standpoint. Architects may prefer brick walls with thickness 37 cm, and limit the thickness of high concrete walls to 45 cm.

6.2. Effect of porosity P_o

Fig. 8 shows the effect of the porosity on the thermal performance of the LPSHW. In addition to the parameters mentioned in the last section and given in Table 1, some other parameters in Fig. 8 are $h=6$ cm, $l=37$ cm for the brick walls, and $l=40$ cm for the concrete walls. Generally, there is an optimum porosity with a normal height wall and a low brick wall. For walls with the same material, the optimum porosity decreases with increasing their heights.

Since the optimum porosity of a low brick wall is almost the same as that of a low concrete wall, it is deduced that thermal conductivity has little effect on the value of the optimum porosity of walls.

6.3. Effect of glazing layer number

The thermal performance improves greatly when the glazing layer number increases from 1 to 2 (Figs. 7 and 8). Therefore, multiple-glazing seems to be an attractive alternative to using night insulation. The heating performance may not be quite as good, but the cost, and especially the operating complexity, can be reduced considerably.

6.4. Effect of night insulation R-value

Fig. 9 shows the effect of the night insulation on the thermal performance of the LPSHW. Some other parameters in the figure are concrete material, $H=1$ m, $h=6$ cm, $P_o=0.4$, and single glazing. It is seen that the night insulation greatly influences the heating performance when the R-value is less than 1.5 m^2 °C W^{-1}.

6.5. Effect of vent height h

Fig. 10 shows the effect of the vent height on the thermal performance of the LPSHW. Some other parameters in the figure are $P_o=0.4$ for the 1-m-high concrete wall, $P_o=0.35$ for the 3-m-high concrete wall, single glazing, $l=40$ mm, and $R=1.5$ m^2 °C W^{-1}. It is seen that the heating performance improves with the vent height decreasing. For a wall constructed with blocks like bricks, h should be greater than 6 cm. Besides, it is not easy to clean dust on the vent surfaces if h is too small.

7. OPTIMUM STRUCTURAL PARAMETERS

Based on the sensitivity analysis, the optimum structural parameters of the LPSHW used in dwelling passive solar heated buildings are as follows: $l=37$ cm for brick walls; $l=35$–40 cm

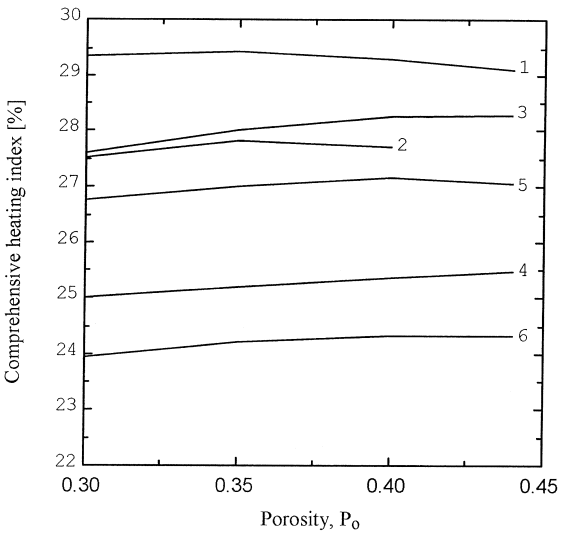

Fig. 8. Effect of porosity on thermal performance.

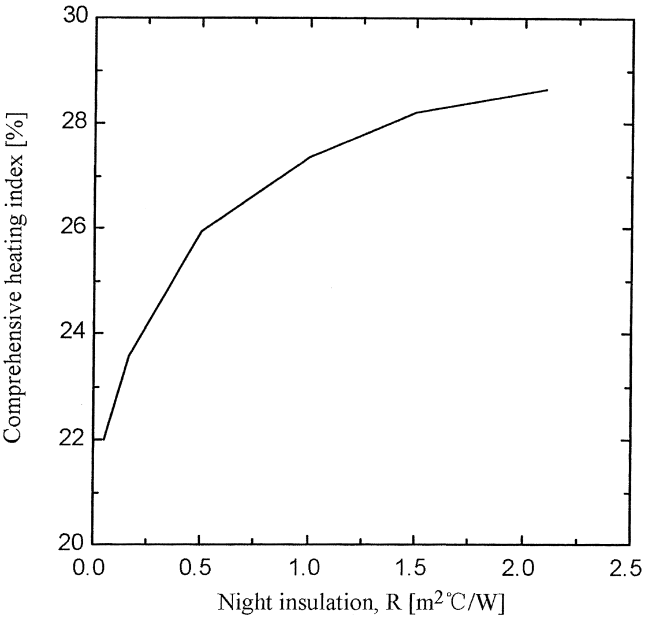

Fig. 9. Effect of night insulation on thermal performance.

for low concrete walls; $l=40$–45 cm for high concrete walls; $P_o=0.35$ for normal height walls; $P_o=0.4$ for low walls; $h=6$ cm.

8. COMPARISON WITH THE TROMBE WALL

The comparison between the LPSHW and the Trombe wall is made under their optimum wall structural parameters with the same other conditions, which are concrete wall, single glazing, $H=1$ m, $R=0.33$ m^2 °C W^{-1}, LCR$=2.4$ W m^{-2} °C^{-1}, and the middle clear solar/weather conditions in Beijing in January.

Under the chosen conditions, the thermal efficiencies are 30.2% for the LPSHW, and 22.6% for the Trombe wall. In addition, the concrete consumption decreases by 35% when using the lattice wall instead of the Trombe wall. Therefore, the LPSHW has advantages over the Trombe wall.

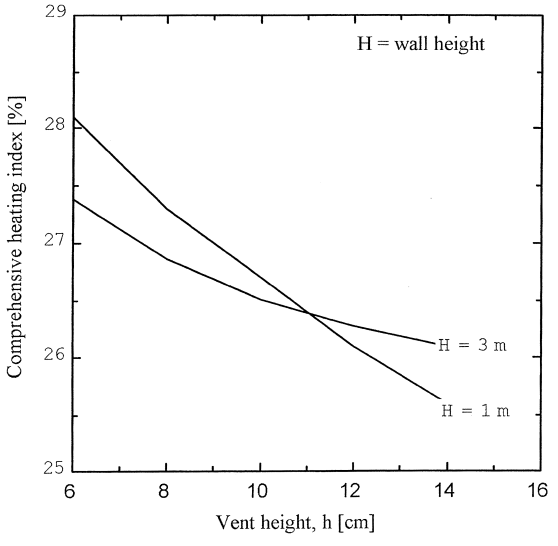

Fig. 10. Effect of vent height on thermal performance.

9. CONCLUSIONS

The mathematical mode of lattice-wall passive solar heated buildings is developed, considering three-dimensional heat conduction in lattice walls.

A computer simulation program in FORTRAN language is worked out based on the mathematical model of lattice-wall passive solar heated buildings, and verified with experimental data. The model predictions agree quite well with the experimental data. The program can be used to simulate and evaluate the transient thermal performance, to analyze the sensitivity and the effect of climate, and to optimize the LPSHW configuration.

Hour-by-hour calculations are run and repeated many times with structural parameters changed one at a time to analyze the sensitivity of the LPSHW. The effect of the glazing layer number, wall height H, night insulation value R, wall thickness l, vent height h, and porosity P_o on the thermal performance of the LPSHW are demonstrated. From the sensitivity analysis, the optimum

structural parameters of the LPSHW are obtained.

The comparison between the LPSHW and the Trombe wall is carried out under their optimum wall structural parameters with the other parameters held the same. The results show that the LPSHW has advantages over the Trombe wall. Under the chosen conditions, thermal efficiency is 30.2% for the LPSHW and 22.6% for the Trombe wall.

NOMENCLATURE

a thermal diffusivity of a lattice wall, m^2/h
$A(i,j,k)$ weight of nodal point (i,j,k) for calculating average radiation temperatures
c specific heat of a lattice wall, J/kg °C
C_d air discharge coefficient of vents, dimensionless
CHI comprehensive heating index, dimensionless
F_0 $a\Delta\tau/l^2$ = Fourier number, dimensionless
g 9.8 m/s^2, acceleration of gravity
h height of a lattice wall element, the same as the height of a lattice wall vent (see Fig. 1b), m if not pointed out
H height of a lattice wall, m
h_{nc} convection heat transfer coefficient of $x = l$ side, W/m^2 °C
h_{nr} radiation heat transfer coefficient of $x = l$ side, W/m^2 °C
h_{sc} convection heat transfer coefficient of $x = 0$ side, W/m^2 °C
h_{sr} radiation heat transfer coefficient of $x = 0$ side, W/m^2 °C
h_{vc} convection heat transfer coefficient of vent surfaces, W/m^2 °C
h_{vgr} radiation heat transfer coefficient of vent surfaces to glazing cover, W/m^2 °C
h_{vwr} radiation heat transfer coefficient of vent surfaces to the interior surfaces of room envelope, W/m^2 °C
I_x solar radiation flux absorbed by $x = 0$ side, W/m^2
I_{ya} solar radiation flux absorbed by $y = 0$ side, W/m^2
I_{yb} solar radiation flux absorbed by $y = w$ side, W/m^2
I_z solar radiation flux absorbed by $z = h$ side, W/m^2
k row number of lattice wall elements of a lattice wall
l thickness of a lattice wall element, the same as the thickness of the lattice wall (see Fig. 1a), m
L thickness of the channel between the lattice wall and the glazing cover (see Fig. 1a), m
LCR defined by Eq. (25), W/m^2 °C
M total rows of lattice wall elements of a lattice wall
$\dot{M}_c$ air mass flow rate at the position Z of the channel between the lattice wall and the glazing cover, kg/m^2 s
$\dot{M}_v$ air mass flow rate of the lattice wall vents with relative altitude Z, kg/m^2 s
Nx total nodal points in x direction
P_o porosity of a lattice wall (see Eq. (23)), dimensionless
$q_{T_{ex}}$ heat supplied at the time when the extreme room temperature occurs, W/m^2
$q_{T_{ex-1}}$ heat supplied at the time 1 h before the extreme room temperature occurs, W/m^2
R night insulation, m^2 °C/W
$T(x,y,z)$ temperature at point (x,y,z) of a lattice wall element, K
T_c temperature of air in the channel between lattice wall and glazing cover, K
T_g temperature of the interior surface of glazing cover, K
T_r room temperature, K
T_v temperature of air in vents of a lattice wall, K
T_w temperature of the interior surfaces of room envelope, K
$\bar{T}_c$ average temperature of air in the channel between lattice wall and glazing cover, K
$\bar{T}_{l-g}$ average radiation temperature of a lattice wall for calculating the interior temperature nodal point of the glazing cover, K
$\bar{T}_{l-r}$ average radiation temperature of a lattice wall for calculating the interior temperature nodal point of the building envelope, K
$\bar{T}_v$ average radiation temperature of vent surfaces of a lattice wall, K
$\bar{T}_{x=0}$ average radiation temperature of $x = 0$ surfaces of a lattice wall, K
$\bar{T}_{x=l}$ average radiation temperature of $x = l$ surfaces of a lattice wall, K
v length in y direction except for the isolated surfaces (see Fig. 1b), m
w width of a lattice wall element (see Fig. 1b), m
Z relative altitude of a given position to the lattice wall bottom, m

Greek symbols

λ thermal conductivity of a lattice wall, W/m °C
ρ density of a lattice wall, kg/m^3
$\rho_{Z=H/2}$ density of air at $Z = H/2$ of the channel between lattice wall and glazing cover, kg/m^3
τ time, h
η thermal efficiency (see Eq. (24)), dimensionless

Superscript

λ parameter at time $n\Delta\tau$, i.e. at the last time nodal point.

APPENDIX A. Summary of the air flow model

The air mass flow rate in the channel between the lattice wall and the glazing cover can be calculated by (Fang, 1984)

$$\dot{M}_c = \pm C_d \rho_{Z=H/2} \frac{P_o h}{L} \frac{\sqrt{Hg}}{4X} \times \left[1 - \left(\frac{2}{H}\left|\frac{H}{2} - Z\right|\right)^{3/2}\right] \sqrt{\frac{|\bar{T}_c - T_r|}{\bar{T}_c}} \quad (A.1)$$

where '+' for $\bar{T}_c - T_r \geq 0$, '−' for $\bar{T}_c - T_r \leq 0$, and

$$X = \begin{cases} 1/\left[(1 + H/h)\sqrt{1 - h/H}\right] & M = \text{odd number} \\ h/H\sqrt{1 - h/H} & M = \text{even number} \end{cases} \quad (A.2)$$

The air mass flow rate of the lattice wall vents with relative altitude Z can be calculated by

$$\dot{M}_v = \pm C_d \rho_{Z=H/2} \frac{\sqrt{Hg}}{4X} \left| \left(\frac{2}{H}\left|\frac{H-h}{2} - Z\right|\right)^{3/2} - \left(\frac{2}{H}\left|\frac{H+h}{2} - Z\right|\right)^{3/2} \right| \sqrt{\frac{|\bar{T}_c - T_r|}{\bar{T}_c}} \quad (A.3)$$

where '+' for $\bar{T}_c - T_r \geq 0$, '−' for $\bar{T}_c - T_r \leq 0$, and X is given by Eq. (A.2).

APPENDIX B. Average radiation temperatures

The weighted average method, with the related nodal point area as the weight, is used to determine the average radiation temperatures. Based on this method, referring to Fig. 2a, the average radiation temperatures of the $x = 0$ and $x = l$ surfaces of a lattice wall are as follows, respectively:

$$\bar{T}_{x=0} = \frac{1}{Mhw}\sum_{k=1}^{M}\sum_{j=1}^{5} A(1,j,k)T(1,j,k) \tag{B.1}$$

$$\bar{T}_{x=l} = \frac{1}{Mhw}\sum_{k=1}^{M}\sum_{j=1}^{5} A(N_x,j,k)T(N_x,j,k) \tag{B.2}$$

The average radiation temperature of vent surfaces of a lattice wall is of the form

$$\begin{aligned}\bar{T}_v = \frac{1}{2Ml(h+w)}\sum_{k=1}^{M}\sum_{i=1}^{N_x}[&A(i,1,k)T(i,1,k)\\ &+ A(i,2,k+1)T(i,2,k+1)\\ &+ A(i,3,k)T(i,3,k)\\ &+ A(i,4,k-1)T(i,4,k-1)]\end{aligned} \tag{B.3}$$

The average radiation temperatures of the lattice wall surfaces for calculating the interior temperature nodal point of the glazing cover and the building envelope are given by Eqs. (B.4) and (B.5), respectively

$$\bar{T}_{l-g} = \frac{1}{w+v}(w\bar{T}_{x=0} + v\bar{T}_v) \tag{B.4}$$

$$\bar{T}_{l-r} = \frac{1}{w+v}(w\bar{T}_{x=l} + v\bar{T}_v) \tag{B.5}$$

REFERENCES

Balcomb J. D., Hedstrom J. C. and MeFarland R. D. (1977). *Passive Solar Heating of Buildings*, LA-UR-77-1162.

Carter C. (1990) Computational methods for passive solar simulation. *Solar Energy* **45**(6), 379.

Crank J. and Nicolson P. (1947) A practical method for numerical evaluation of solutions of partial differential equations of the heat-conduction type. *Proc. Cambridge Phil. Soc.* **43**, 50.

Fang X. D. (1984). *Experimental Optimization and Mathematical Simulation of Lattice Passive Solar Heating Walls*, Tsinghua University, Beijing, China, Thesis.

Fang X. D. (1986) Research into solar test cells. *Acta Energiae Solaris* **7**(1), 80.

Incropera F. P. and DeWitt D. P. (1996). In *Fundamentals of Heat and Mass Transfer*, p. 493, John Wiley, New York.

Li Y. Z., Di H. F. and Fang X. D. (1989). *Fundamental and Design of Passive Solar Heated Buildings*, Energy Press, Beijing.

Li Y. Z. and Fang X. D. et al. (1985) Experimental research and residential applications of the lattice solar wall. In *Proceedings of International Conference on Solar and Wind Energy Applications, August 3–7, Beijing, China*.

Li Y. Z., Zhao S. H. and Zhang J. Z. (1983) The optimization of a compound passive solar house. *Acta Energiae Solaris* **4**(2), 117.

Metais B. and Eckert E. R. G. (1964) Forced, mixed and free convection regimes. *J. Heat Transfer* **86**, 295.

Roache P. J. (1972). In *Computational Fluid Dynamics*, p. 91, Hermosa Publishers.

Utzinger D. M. et al. (1968) The effect of air flow rate in collector-storage wall. *Solar Energy* **25**, 511.

Welty J. R. (1978). *Engineering Heat Transfer*, John Wiley, New York.